

A THERMO-HYGRO-MECHANICAL MODEL FOR CONCRETE SHRINKAGE: PRELIMINARY STUDY

1. Introduction and scope

The concrete shrinkage is a common effect of the concrete material behavior during concrete strengthening. The shrinkage is usually a function of the particular concrete material features, its quality, curing process, structural element size, and thermal-hydraulic boundary conditions during the working stress life-time conditions. Typically, grid-geometry steel bars with reinforcement function (rebar) are placed close to the concrete contour surface (coating spacing) to avoid the undesired shrinkage cracks with consequent material section loss. In addition to the solution through classical steel-grid rebar, there are other alternatives considering new materials and methodologies during concrete casting which are still under development (as the use of master fibers is) and may be also appropriate to avoid concrete shrinkage cracking with reducing material and installation costs.

In order to analyze the concrete shrinkage problem and improve the knowledge of the tensile stress loss at the zone close to the structural element contour facing, a numerical 2D finite element method (FEM) Thermo-Hygro-Mechanical (THM) model was developed. The FEM software used was CODE_BRIGHT (Olivella *et al.* 1996) which uses the GID pre- and post-processor software (GID-CIMNE 2017), both developed at the Universitat Politècnica de Catalunya – BarcelonaTech and the International Center for Numerical Methods in Engineering (DECA-UPC / CIMNE 2017).

At this stage, this first model and achieved results were only attempted to be of interest at a qualitatively level. Further tests may be appropriate to, first, identify and properly fix material parameter values which were here approximate, and second, to verify and validate the reached learnings and obtained stress-strain behavior results.

2. Model features and material properties

A plain-strain finite element 2D model was generated with dimensions of 2.0 m-long \times 0.2 m-thick plate geometry (see **Figure 1**). The 2D FEM model mesh presented is composed by 1000 hexahedral elements, generating 1066 nodes.

Two different model cases were considered, one assuming plain concrete (i.e., mass concrete with no reinforcement) and another one assuming steel grid reinforcement with 10 mm-diameter. As shown in **Figure 1**, the same mesh was used for both modelled cases (i.e., plain and reinforced concrete).

Table 1 presents the material properties considered. Concrete was treated as an elastic-plastic material with a Drucker Prager failure criterion (cone shape proportional to confinement) with strength parameters basically defined by an inter-particle friction angle (ϕ) and a shear strength

value at zero normal stress (c), which is independent of ϕ . Shrinkage is represented proportional with suction variation (due to drying process).

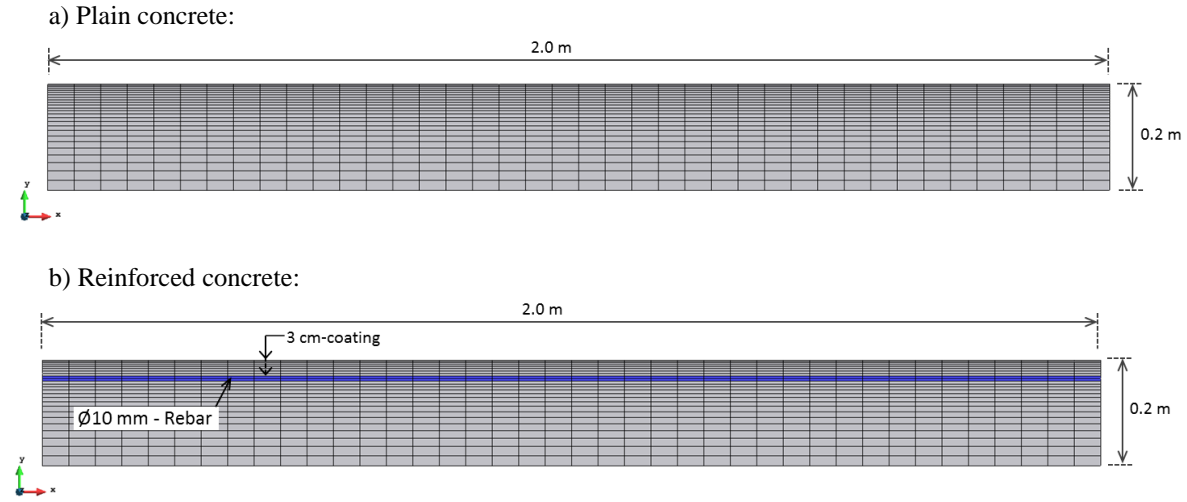


Figure 1. Model geometries and boundary conditions on displacements: (a) Plain concrete and (b) Reinforced (Rebar) concrete case studies.

Table 1. Material properties.

	Properties	Concrete	Steel rebar
Phase:	Unit weight, γ (kN/m ³)	23.5	78.5
	Initial Porosity, ϕ (-)	0.145	0.0001
Elastic:	Elastic Modulus, E (MPa)	25000	210000
	Poisson's ratio, ν (-)	0.15	0.3
	Shrinkage coefficient for suction changes, a_s (MPa ⁻¹)	0.0001	-
Plastic:	Interparticle friction angle, ϕ (deg.)	38	-
	Shear strength independent to friction, c (kPa)	200	-
	Dilatancy angle, ψ (deg.)	38	-
Hydraulic and Thermal ^(a) :	Retention curve: Van Genuchten:		
	P_1 ^(b) (MPa)		0.1
	Shape function (-)		0.5
	Intrinsic permeability, k_{ij} (m ²)		5.0×10^{-19}
	Relative permeability k_r -power (-)		3
	Heat flux conductivity:		
	Dry, λ_{dry} (W/mK)		1.0
	Saturated, λ_{sat} (W/mK)		1.5

Notes: ^(a) despite the hydraulic and thermal properties of the steel and the concrete are different, the same ones assumed for the concrete were also assumed at the steel-rebar occupied geometry. This better suits the steel-grid 2D geometry, were most of the domain is concrete material instead of steel (which in this case just provides mechanical features to the whole structural domain);

^(b) atmospheric pressure (approximate).

With regards to the boundary conditions, a prescribed relative humidity of 0.65 (i.e., RH = 65%) was assigned to the top surface contour whereas the whole concrete sample was assumed to be initially saturated (RH = 100%, Liquid pressure = 0.1 MPa). Bottom and lateral side contours were assumed to not include any mass flux. The assumed initial temperature was 20°C to all defined domain (temperature assumed almost constant in these case studies). **Figure 2** presents a schematic representation of the boundary conditions. The interval calculation time was up to 28 days.

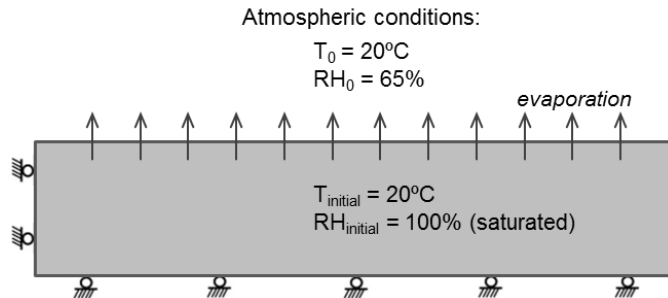


Figure 2. Schematic representation of the boundary conditions considered.

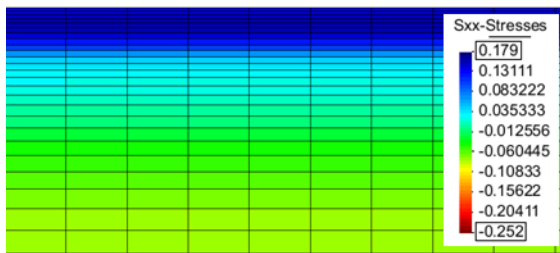
3. Results

Figure 3 presents results of the horizontal stress development at the end of the calculation (i.e., after 28 days of atmospheric boundary conditions application) through the vertical cross-section of the sample at the central part of the structure (i.e., at about $x = 1.0$ m from the lateral contour of the structure).

As it can be noticed, first, fixing the minimum and maximum ranging values, different distribution of stresses was reached between the plain concrete (left) and the reinforced concrete (right) cases. The top surface tension stresses generated were similar between both cases, reaching about 160-180 kPa. At the bottom contour, about 80 kPa compression stress was reached for the plain concrete case in front of the 250 kPa reached for the reinforced concrete case (values below concrete tensile strength). The explanation of these different results is, as the integral of the stress developed through the vertical section should remain equal between both cases (there is no external loads, so all stresses have to be generated from the same defined elements), the reinforcement element should to generate the equivalent tensile stresses, absorbing (by shear) part of the tensile stresses developed at the top zone of the sample (see **Figure 3b**-bottom).

The stress values reached are strictly related to the input material parameters chosen, which have not been experimentally confirmed. Thus, only qualitative (i.e., not quantitative) learnings can be done at this stage.

a) Plain concrete:



b) Reinforced concrete:

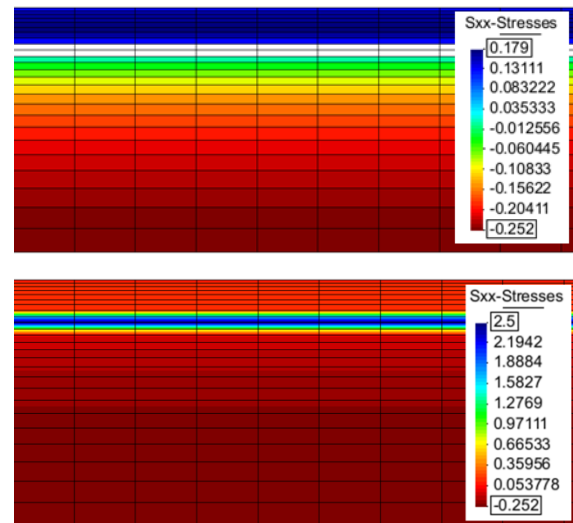


Figure 3. Horizontal x-stress development after 28 days: (a) Plain and (b) Reinforced concrete with and without steel rebar display selected (top and bottom, respectively; see ranging values).

Figure 4 presents the horizontal stress vector results for plane and reinforced concrete cases after 7, 14, 21, and 28 days. As it can be seen, different distribution and magnitude of the vectors were obtained (the same vector size factor was assumed between both cases). Different depths of tensile stresses were obtained between the two cases, and only concrete compression was developed below the rebar at the x-direction after 20 days due to the reinforcement strength.

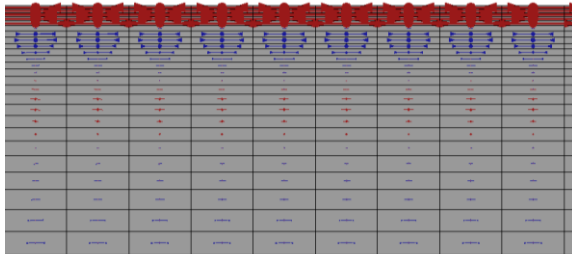
Figure 5 presents the evolution of the horizontal stresses for several points through the vertical cross-section of the sample's thick. In a glance, despite the trending oscillations (which can be attributed to numerical issues), similar trends were obtained. However, slightly downward slope trend was obtained at the compression stress points (bottom-half of the sample) in the reinforced concrete case whereas a more horizontally-stabilized trend was obtained a for the plain concrete case at the same points. **Figure 6** presents horizontal stress evolution of the top-half points between both cases. Despite slightly different trending evolution was achieved in some points at initial times, no much difference was obtained at the end of calculation with resulting stabilized tensile stresses ranging between 140-150 in plain concrete and 150-180 kPa in reinforced concrete case.

Figure 7 presents the resulting volumetric and deviatoric plastic strains at 28 days evolution in both cases. As it can be observed, no significant differences were obtained (note that the same ranging values were fixed for shown results in both cases). According to this non-relevant difference between plain and reinforced concrete strain results, in **Figure 8**, the volumetric plastic strains at 7, 14, 21, and 28 days are shown for the reinforced concrete (rebar) case only. Volumetric plastic strains evolution results in an increase of the plastic zone proportionally to the time. Similar results were obtained for the deviatoric plastic strains evolution. In both cases (i.e., plain and reinforced

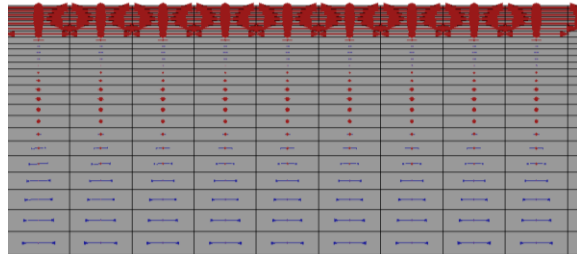
concrete), the plastic strains did not reach the depth level of the reinforcement location (or equivalent depth in the plain concrete case).

a) Plain concrete:

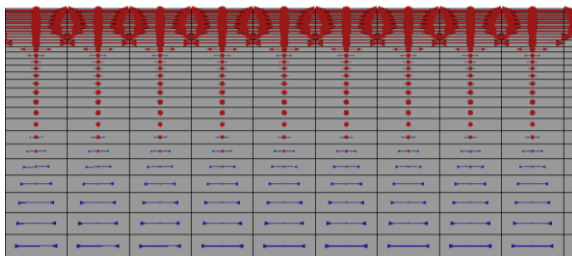
7 days



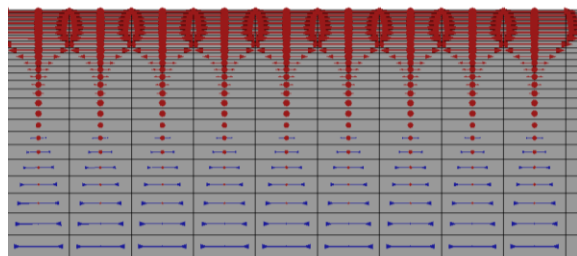
14 days



21 days



28 days

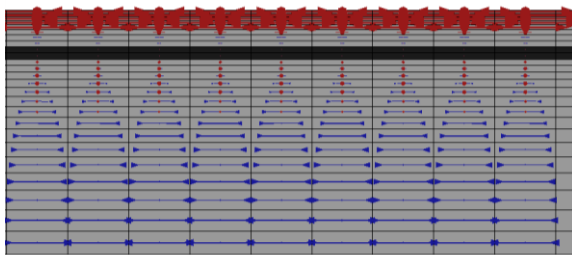


Display Vectors of Stresses, All factor 0.5.

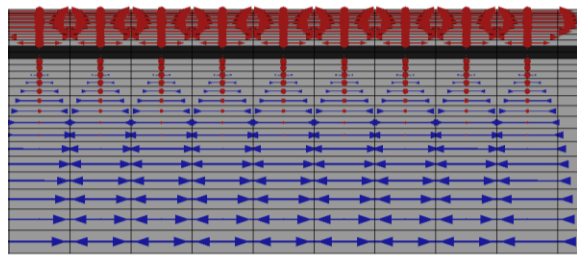


b) Reinforced concrete:

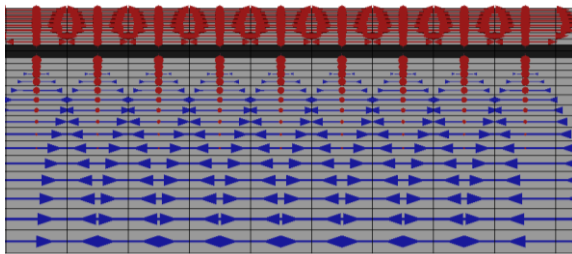
7 days



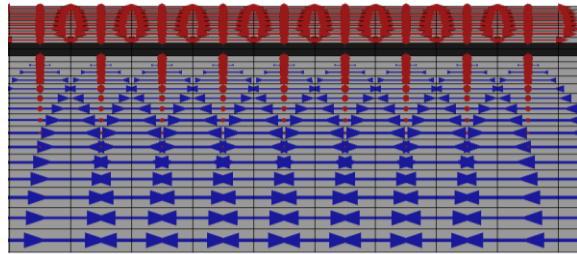
14 days



21 days



28 days

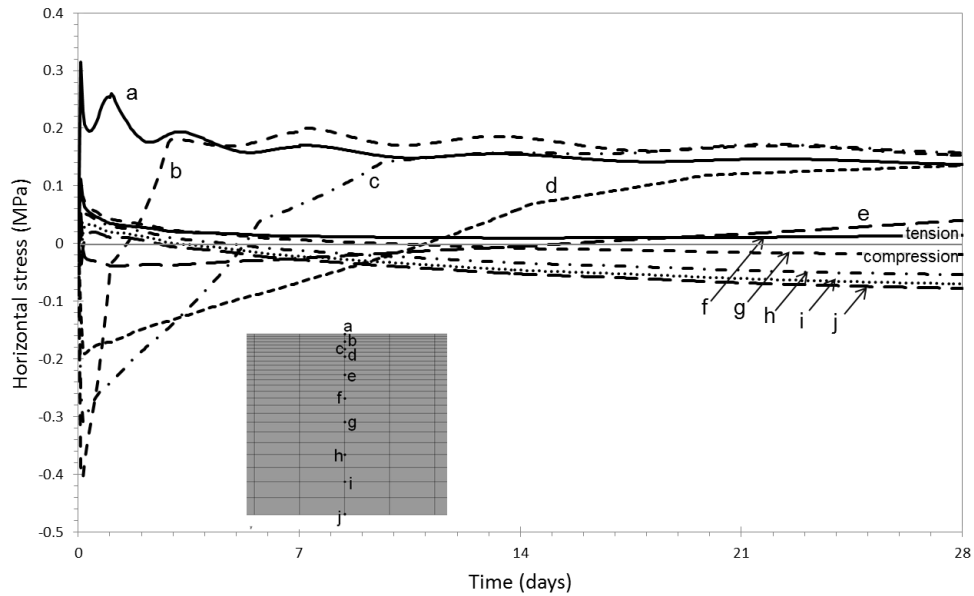


Display Vectors of Stresses, All factor 0.5.



Figure 4. Main stress vectors after 7, 14, 21, and 28 days: (a) Plain and (b) Reinforced concrete cases.

a) Plain concrete:



b) Reinforced concrete:

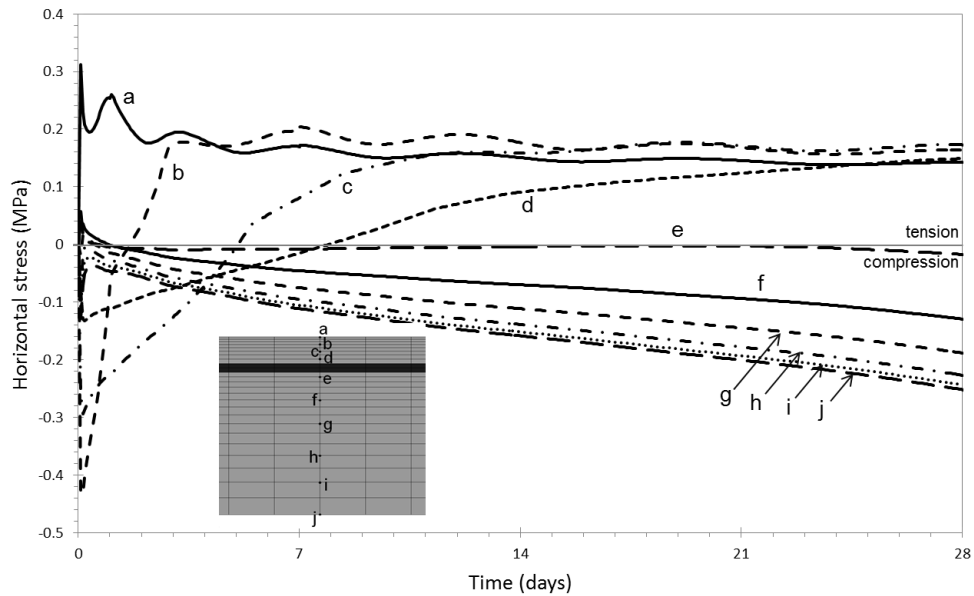


Figure 5. Horizontal stress development at several cross-section points in the middle of the sample ($x=1.0$ m): (a) Plain and (b) Reinforced concrete cases.

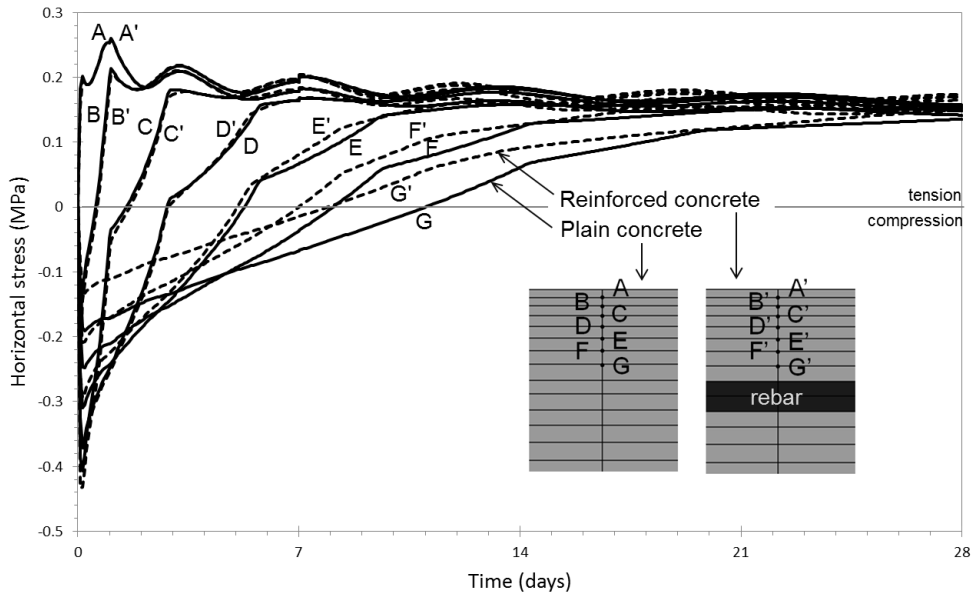
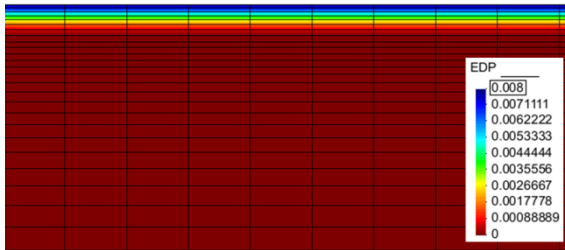
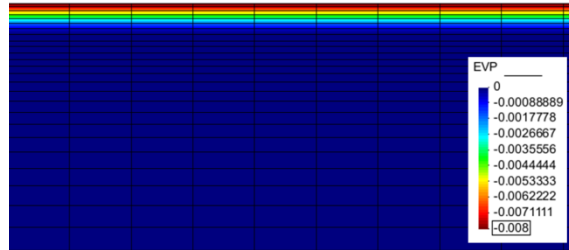


Figure 6. Horizontal stress development at several points on top of the sample (at $x=1.0$ m): Plain and Reinforced concrete comparison results.

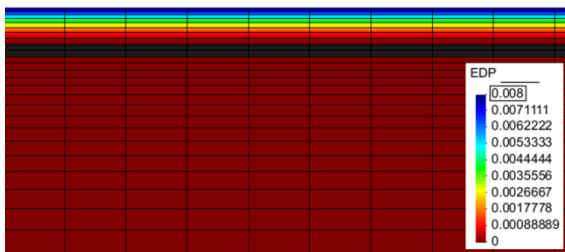
a) Plain concrete:
 Deviatoric:



Volumetric:



b) Reinforced concrete:
 Deviatoric:



Volumetric:

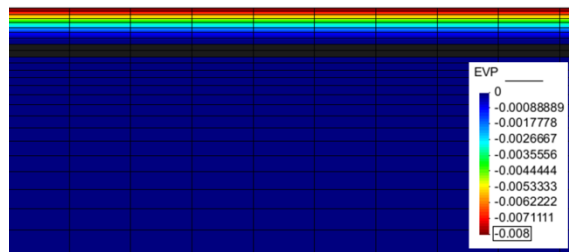


Figure 7. Deviatoric and volumetric plastic strains development after 28 days: (a) Plain and (b) Reinforced concrete cases.

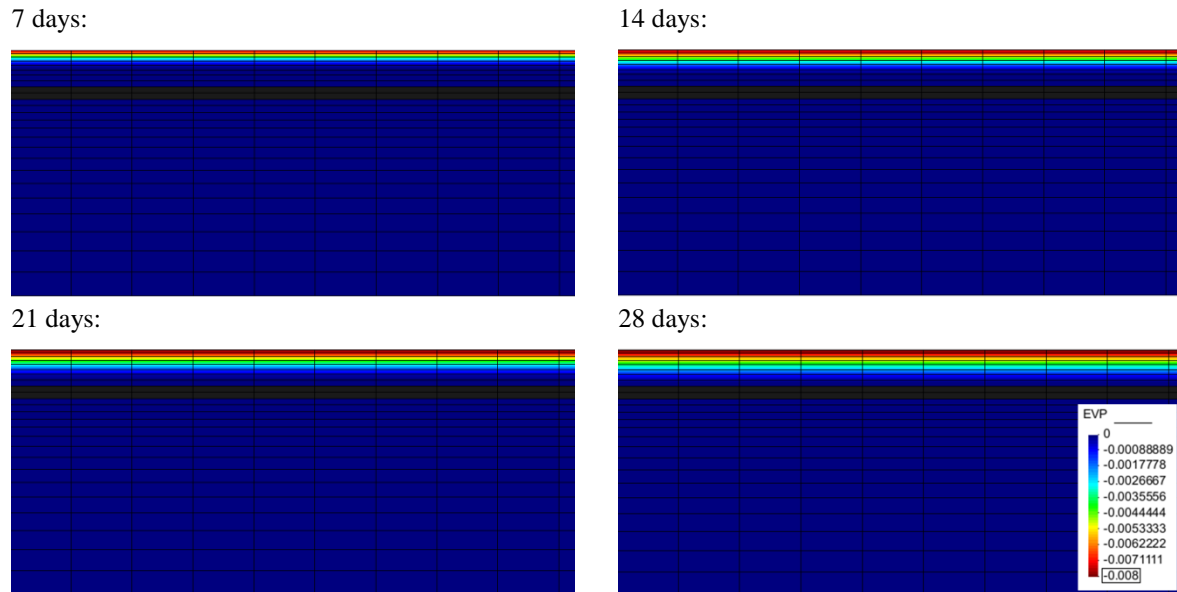


Figure 8. Volumetric plastic strains development after 7, 14, 21, and 28 days for Reinforced concrete case.

The variation of the relative humidity generated is presented in **Figures 9** and **10**. The same control points at the top of the sample as in **Figure 6** are analyzed in **Figure 10**. As it can be observed similar trends were obtained between both cases. However, somewhat faster loose of humidity occurred in the plain concrete case.

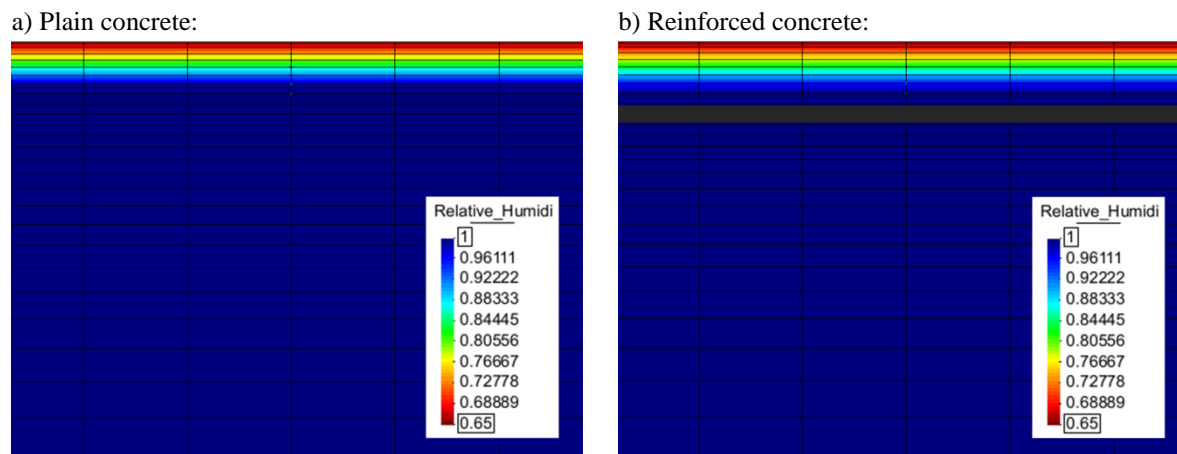


Figure 9. Relative humidity development: (a) Plain and (b) Reinforced concrete cases.

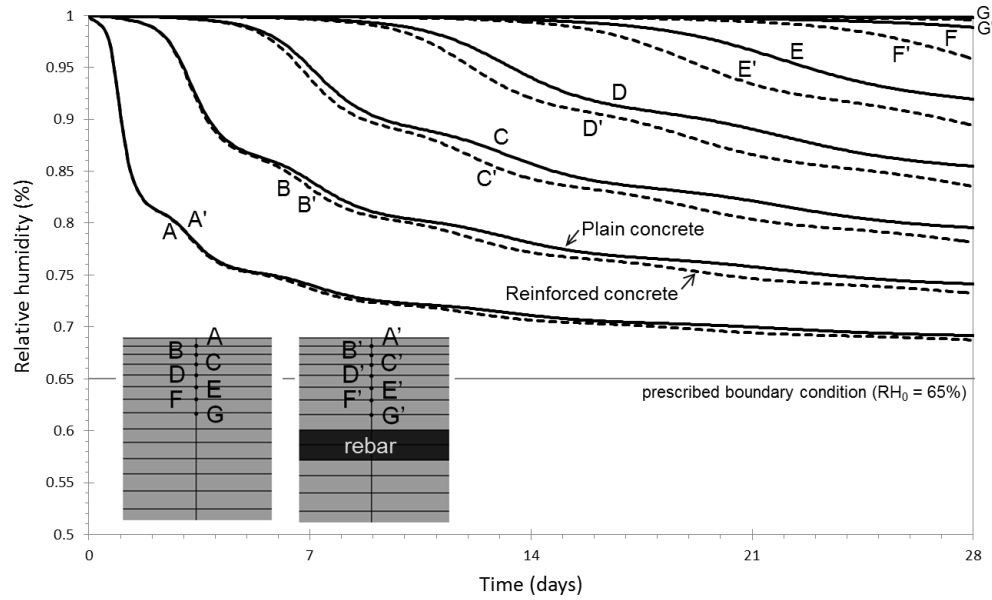


Figure 10. Relative humidity development at several points on top of the sample (at $x=1.0$ m): Plain and Reinforced concrete comparison results.

4. Conclusions

The achieved results and presented methodology look promising to reach a full set of sensitivity analyses regarding the reinforced concrete material features and geometry:

- The constitutive material model selected at this stage may require further improvements with more accurate concrete material features. The proper model implementation may require real shrinkage full-scale tests in order to determine more realistic thermal and hydraulic plain concrete material properties as the ones assumed at this first-attempt modelling stage.
- In terms of the geometry variations, both coating spacing and rebar diameter may be analyzed.
- A 3D modelling may be developed in order to perform real grid-rebar geometry cases and to identify possible variations due to the real concrete-to-concrete contact instead of the actual 2D plane-strain assumed simplification.

A proper calibration is strongly required in order to make results representative and in line with reality. Volume contraction values from full-scale sample tests would provide valuable information of the THM process analyzed, with a proper data acquisition of the relative humidity and temperature of the sample and surrounding environment during tests development. All this above would provide information to calibrate main parameters (as the shrinkage coefficient for suction changes) allowing the validation/verification of the model and obtained results.

5. References

CODE_BRIGHT, DECA-UPC / CIMNE, 2017. Department of Civil and Environmental Engineering (School of Civil Engineering), Universitat Politècnica de Catalunya / International Center for Numerical Methods in Engineering.

https://deca.upc.edu/ca/el-departament/seccions/etcg/recerca/projectes/code_bright

<https://www.gidhome.com/gid-plus/modules/modules-research/27/codebright/>

GID-CIMNE, 2017. GID - The personal pre and post processor. <https://www.gidhome.com>

Olivella, S., Gens, A., Carrera, J., and Alonso, E.E., 1996. Numerical formulation for a simulator (CODE-BRIGHT) for the coupled analysis of saline media. *Engineering Computations* 1: 87– 112.